JOURNAL OF GEOPHYSICAL RESEARCH, VOL. 115, D04205, doi:10.1029/2008JD010868, 2010

Predicting the potential for lightning activity in Mediterranean storms based on the Weather Research and Forecasting (WRF) model dynamic and microphysical fields

Yoav Yair,[1] Barry Lynn,[1,2] Colin Price,[3] Vassiliki Kotroni,[4] Konstantinos Lagouvardos,[4] Efrat Morin,[5] Alberto Mugnai,[6] and Maria del Carmen Llasat[7]

Received 29 July 2008; revised 7 August 2009; accepted 29 September 2009; published 27 February 2010.

[1] A new parameter is introduced: the lightning potential index (LPI), which is a measure of the potential for charge generation and separation that leads to lightning flashes in convective thunderstorms. The LPI is calculated within the charge separation region of clouds between 0°C and −20°C, where the noninductive mechanism involving collisions of ice and graupel particles in the presence of supercooled water is most effective. As shown in several case studies using the Weather Research and Forecasting (WRF) model with explicit microphysics, the LPI is highly correlated with observed lightning. It is suggested that the LPI may be a useful parameter for predicting lightning as well as a tool for improving weather forecasting of convective storms and heavy rainfall.

Citation: Yair, Y., B. Lynn, C. Price, V. Kotroni, K. Lagouvardos, E. Morin, A. Mugnai, and M. d. C. Llasat (2010), Predicting the potential for lightning activity in Mediterranean storms based on the Weather Research and Forecasting (WRF) model dynamic and microphysical fields, *J. Geophys. Res.*, *115*, D04205, doi:10.1029/2008JD010868.

1. Introduction

[2] The complex relationships between lightning and rain yields in convective storms have been studied extensively, with different relationships derived in varying geographical locations and atmospheric conditions. The early work of *Piepgrass et al.* [1982] identified different regimes with specific rain yield per flash ratios for each regime. *Petersen and Rutledge* [1998] computed the ratios of area mean rainfall and cloud-to-ground (CG) lightning flash density for various locations on a temporal scale of 1 month and spatial scales of 10^4–10^5 km^2. They found that values ranged from $\sim 10^8$ kg/fl (where fl denotes flash) in most of the continental United States and tropical continental areas to a value of 10^{10} kg/fl in the Pacific Ocean. More recently, *Gungle and Krider* [2006] presented tables summarizing numerous previous studies that tried to derive the relationships of precipitation volume per lightning flash from different sensors, such as rain gauges and radar. The lag time between lightning and surface rainfall varied from 4–20 min based on rain gauges to <10 min based on radar, with some studies indicating that the first intracloud (IC) activity (IC flashes) occurs almost at the same time when precipitation is observed near the cloud base. The variability of such relationships probably reflects the geographical differences in thunderstorm characteristics, as apparent from the works in the United States by *Tapia et al.* [1998], *Land and Rutledge* [2002], and *Latham et al.* [2003]; in France by *Soula et al.* [1998]; and in China by *Zhou et al.* [2002].

[3] In the Mediterranean region, *Altaratz et al.* [2003], *Defer et al.* [2005], *Price and Federmesser* [2006], and *Katsanos et al.* [2007a, 2007b] studied lightning occurrences and lightning-rainfall relationships, based on satellite (Tropical Rainfall Measuring Mission (TRMM) Lightning Image Sensor (LIS)) and ground-based lightning location systems. Lightning frequency in the eastern Mediterranean seems to peak around November, with a notable preference for maritime over continental lightning activity. Flooding in this region is usually caused by convective storms with rain rates exceeding 50 mm h^{-1} and commonly occurs in autumn. The parent clouds for flash floods are well-developed cumulonimbus clouds, which are also accompanied by intense lightning activity. *Llasat* [2001] showed that the use of the threshold of 50 mm h^{-1} is effective to distinguish between convective and nonconvective rainfall in the context of flash flooding in the Mediterranean coast of Spain.

[4] The microphysical processes that lead to the formation of precipitation particles are also involved in charge separation that leads to the buildup of electric fields in convective clouds. The noninductive mechanism, postulated to be the dominant process, involves rebounding collisions between graupel particles and cloud ice crystals and requires the presence of supercooled liquid water [*Mason and Dash*, 2000; *Mansell et al.*, 2005] (for an updated review of the

[1]Department of Life and Natural Sciences, Open University, Ra'anana, Israel.
[2]Weather It Is, Ltd., Efrat, Israel.
[3]Department of Geophysics and Planetary Science, Tel-Aviv University, Ramat Aviv, Israel.
[4]Institute of Environmental Research, National Observatory of Athens, Athens, Greece.
[5]Department of Geography, Hebrew University of Jerusalem, Jerusalem, Israel.
[6]ISAC, CNR, Rome, Italy.
[7]Department of Astronomy and Meteorology, Faculty of Physics, University of Barcelona, Barcelona, Spain.

0148-0227/10/2008JD010868$09.00

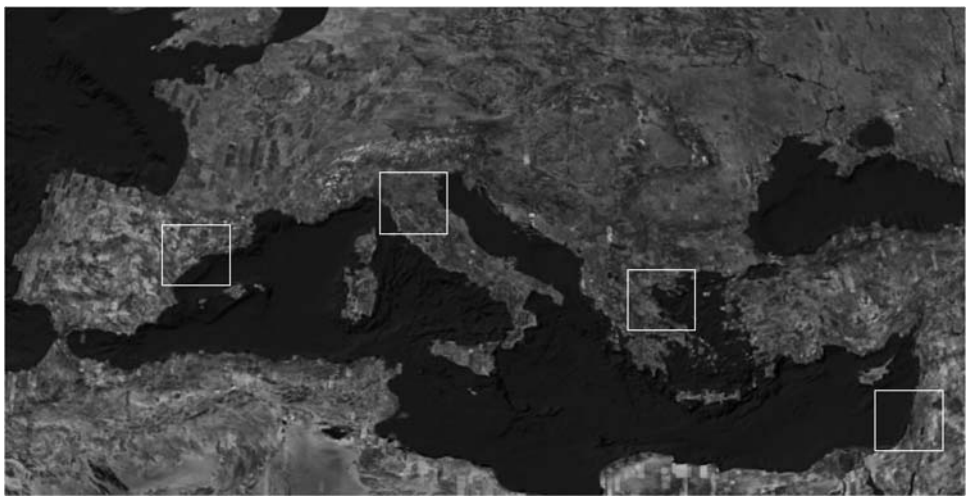

Figure 1. Location of the domains of the five case studies.

microphysics of charge separation, see *Saunders* [2008]). Thus, it is hardly surprising that remote sensing studies find a positive correlation between the presence of precipitating ice in clouds and the intensity of their lightning activity [*Sherwood et al.*, 2006; *Deierling et al.*, 2008].

[5] While the connection between cloud microphysics and lightning seems apparent, the common indices used for forecasting thunderstorms and the potential for lightning mostly rely on stability and thermodynamical indices. The K index (KI) [*Sturtevant*, 1995] was developed to assess the potential for severe thunderstorms. It is a combination of the lapse rate (temperature, T, difference between 850 and 500 hPa), the lower-level moisture content (dew point, T_d, at 850 hPa level), and the moist layer depth, approximated by the difference between the T and T_d at the 700 hPa level. The KI is defined by

$$\mathrm{KI} = (T_{850} - T_{500}) + T_{d850} - (T_{700} - T_{d700}). \qquad (1)$$

The values of KI, which determine the probability for thunderstorms, are given in Appendix A. It should be noted that thermodynamic parameters may serve as a highly discriminating feature for situations in which the synoptic setting fails to explain either atmospheric phenomena or rainfall distribution. This is the case in heavy rainfall situations, where the coexistence of instability and high water vapor content is a critical factor [*Gibergans-Báguena and Llasat*, 2007].

[6] Another index commonly used by meteorologists is the lifted index (LI). In this index, an air parcel is lifted from the surface with temperature and mixing ratios representative of the mean layer values of the lowest 100 hPa of the atmosphere. This hypothetical parcel is then lifted dry adiabatically to the lifting condensation level and pseudo-adiabatically to 500 hPa. The value of this index is the temperature of the environment minus the temperature of the parcel at 500 hPa. The accepted values of the LI indicating the risk of thunderstorms and severe weather are listed in Appendix A.

[7] A new approach was developed by *Bright et al.* [2005], who introduced the concept of Cloud Physics Thunder Parameter (CPTP), based on evidence for the correlations between the presence of ice in the mixed phase region and the level of electrification. The CPTP implies that the convective updraft must be strong enough to ensure supercooled liquid water is replenished and graupel is lifted above the charge reversal temperature zone (-15°C to -20°C [*Saunders et al.*, 1991]); it produces a "plan view" depiction of where thermodynamics support thunderstorms by utilizing the convective available potential energy (CAPE) [*Williams and Renno*, 1993]. It is formulated by

$$\mathrm{CPTP} = (-19^{\circ}\mathrm{C} - T_{\mathrm{EL}})(\mathrm{CAPE}_{-20^{\circ}} - \mathrm{K})/\mathrm{K}, \qquad (2)$$

where T_{EL} is the equilibrium temperature, $\mathrm{CAPE}_{-20^{\circ}}$ is the CAPE between the 0°C isotherm to -20°C, and K is a constant with a value of 100 J kg^{-1}. Although it reflects the correct preconditions for cloud vertical development and accounts for the presence of the cloud in the main charging region, this parameter does not consider the actual microphysical fields involved in cloud electrification.

[8] Many of these parameters or indices can be diagnosed from the observational radiosondes. Likewise, they can be forecasted from numerical weather output [*Davis*, 2001]. Yet, with the advent of high-resolution (e.g., $\sim$3 km) operational weather prediction models, it may be possible to use model output of microphysical parameters in conjunction with the vertical velocity field to parameterize the potential for charge separation that leads to lightning discharge. *Lynn and Yair* [2008] presented preliminary results for this approach, in which they defined the lightning potential index (LPI), which is described in section 2. The results of the present study are presented in section 3, and the summary and conclusions are given in section 4.

2. Methodology

2.1. Lightning Potential Index

[9] We assume that the effective charge separation region within developing thunderstorms is the volume between the freezing level and the -40°C isotherms, where supercooled liquid water can coexist with cloud ice, graupel pellets, and

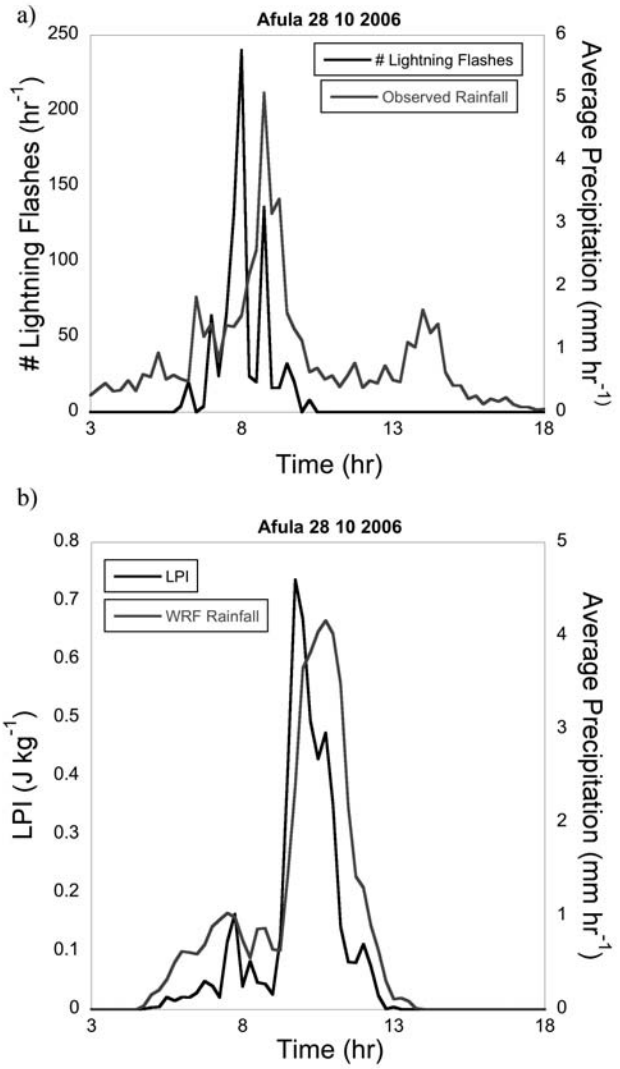

Figure 2. (a) The number of cloud-to-ground (CG) lightning flashes and the radar-derived precipitation as a function of time around the time of peak rainfall. (b) The lightning potential index (LPI) values and Weather Research and Forecasting (WRF)-derived average precipitation for the same time period.

snow crystals. Charge separation occurs via the noninductive ice-graupel mechanism [*Takahashi*, 1978; *Saunders and Peck*, 1998; *Caranti et al.*, 1991]. The electric charge buildup rate is directly proportional to the concentrations of the interacting particles and to the fourth power of the velocity difference between their respective fall speeds [*Keith and Saunders*, 1989]. The LPI is the kinetic energy of the updraft in the developing thundercloud, scaled by the potential for charge separation based on ratios of ice and liquid water within the main "charging zone" (0°C to −20°C) of the cloud. It is calculated using the simulated grid-scale vertical velocity and simulated hydrometeor mass mixing ratios of liquid water, cloud ice, snow, and graupel. This follows on findings by *Deierling and Petersen* [2008] that showed that the updraft volume in the charging zone (at temperatures below −5°C) was highly correlated with total lightning activity. The LPI is nonzero only within the charging zone, and furthermore the LPI for a particular model grid point is only nonzero when a majority of cells within a five-grid radius (10 km) of that grid point have a vertical velocity >0.5 m s^{-1}, indicating the growth phase of the thunderstorm. The LPI (J kg^{-1}) and is defined as

$$\mathrm{LPI} = 1/V \iiint \varepsilon w^2 \mathrm{d}x\mathrm{d}y\mathrm{d}z, \tag{3}$$

where V is the volume of air in the layer between 0°C and −20°C, w is the vertical wind component (m s^{-1}), and q_s, q_i, and q_g are the model-computed mass mixing ratios for snow, cloud ice, and graupel, respectively (in kg kg^{-1}). The integral is computed within the cloud volume from the freezing level (altitude in km above the surface) to the height of the −20°C isotherm; ε is a dimensionless number that has a value between 0 and 1 and is defined by

$$\varepsilon = 2(Q_i Q_l)^{0.5}/(Q_i + Q_l), \tag{4}$$

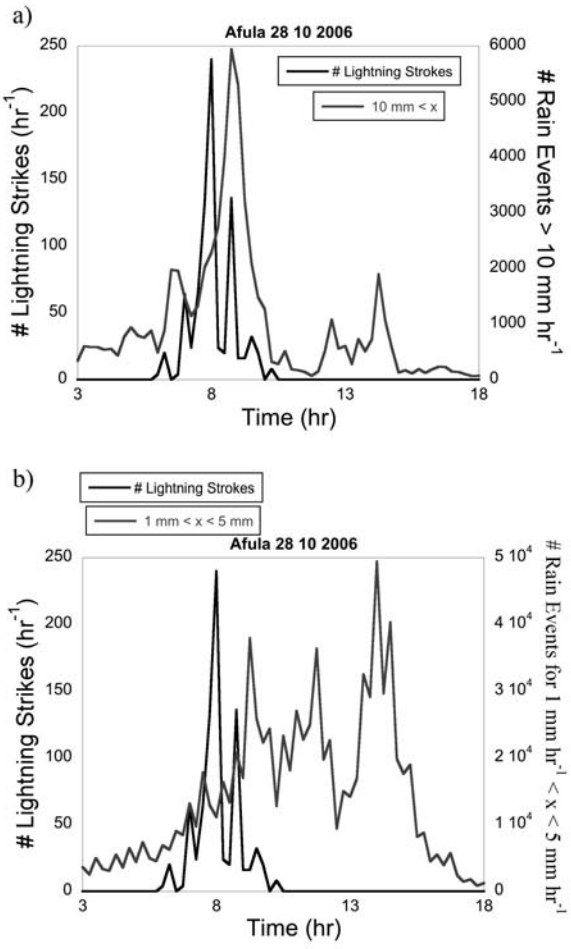

Figure 3. (a) The number of CG lightning flashes versus the number of radar-derived observed rainfall events when the rainfall is >10 mm h^{-1}. (b) The same variables but for rainfall values between 1 and 5 mm h^{-1}. The bounding box was between 34.79°E and 35.79°E, 32.11°N and 33.11°N.

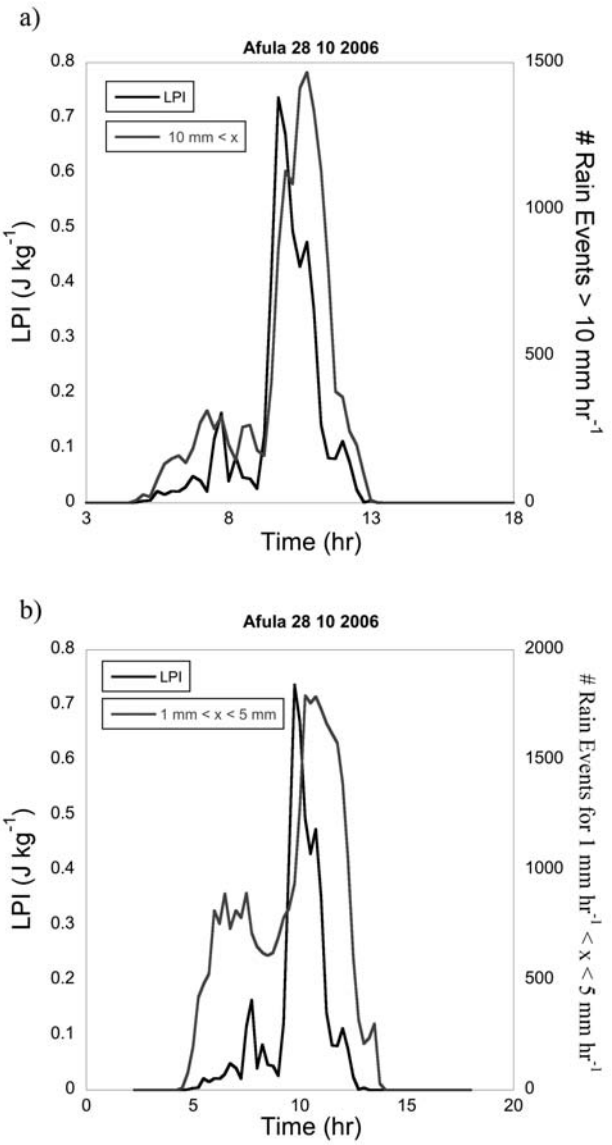

Figure 4. (a) The WRF-derived LPI versus the computed rainfall events when the rainfall is >10 mm h^{-1}. (b) The same variables but for rainfall values between 1 and 5 mm h^{-1}.

where Q_l is the total liquid water mass mixing ratio (kg kg^{-1}) and Q_i is the ice fractional mixing ratio (kg kg^{-1}) defined by

$$Q_i = q_g\left[\left((q_s q_g)^{0.5}/(q_s+q_g)\right)+\left((q_i q_g)^{0.5}/(q_i+q_g)\right)\right]. \quad (5)$$

In essence, ε is a scaling factor for the cloud updraft and attains a maximal value when the mixing ratios of supercooled liquid water and of the combined ice species (the total of cloud ice, graupel, and snow) are equal. It signifies the fact that charge separation requires all these ingredients to operate synergistically within the charging zone, as shown by many laboratory experiments summarized by *Saunders* [2008]. Note that most bulk schemes produce mass information and not number concentration of various hydrometeor types. Hence, we used relative masses of water and ice hydrometeors in our LPI formulation.

[10] The LPI portrays the potential of the thundercloud to separate electrical charge in the 0°C to −20°C depth of the cloud via the noninductive ice-graupel mechanism, but it does not calculate either the electric field or its evolution until it reaches breakdown values. However, the LPI itself does evolve with time since it is calculated from the microphysical and dynamical model fields at each time step and in every domain grid point. Therefore, calculation of the LPI from the cloud-resolving atmospheric model output fields can provide maps of the microphysics-based potential for electrical activity and lightning flashes. As we show in sections 3.1–3.5, this potential correlates well with the actual observed lightning activity, with the inherent limitations of Lightning Position and Tracking System (LPATS)-type systems to detect IC flashes and the imperfect performance of the ZEUS network (and see section 2.3).

2.2. Weather Research and Forecasting Model

[11] The Weather Research and Forecasting (WRF) model [*Skamarock et al.*, 2005] is a fully compressible, nonhydrostatic atmospheric model, using a terrain-following hydrostatic vertical pressure coordinate. It is used by many operational services for short- and medium-range weather forecasting and is also an accessible research tool, as it offers multiple physics options that can be flexibly combined in many ways (the formulation and documentation are available through the University Corporation for Atmospheric Research, and a concise description may be found at http://www.mmm.ucar.edu/wrf/users/pub-doc.html).

[12] The WRF model has many different physics options, which makes it a valuable research module for various applications in various scales. In the present work, version 2.2 was used to explicitly simulate historical flash floods events in the Mediterranean region. The model setup

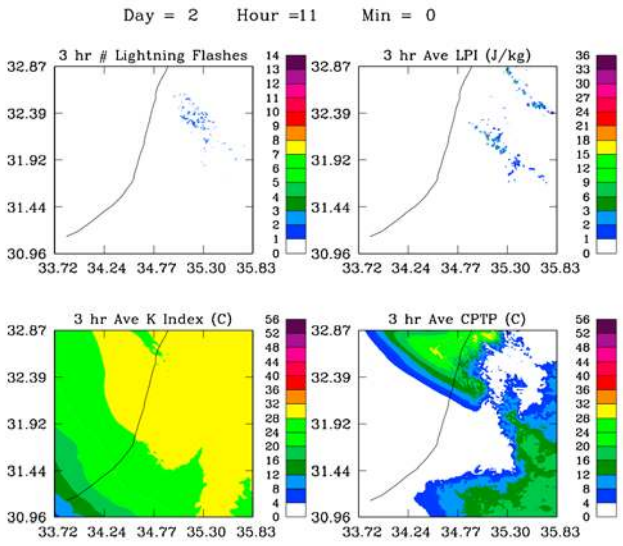

Figure 5. Three hour averages of observed lightning and predicted LPI, K index, and Cloud Physics Thunder Parameter (CPTP) for 0600–0900 UTC on 2 April 2006 (for north central Israel).

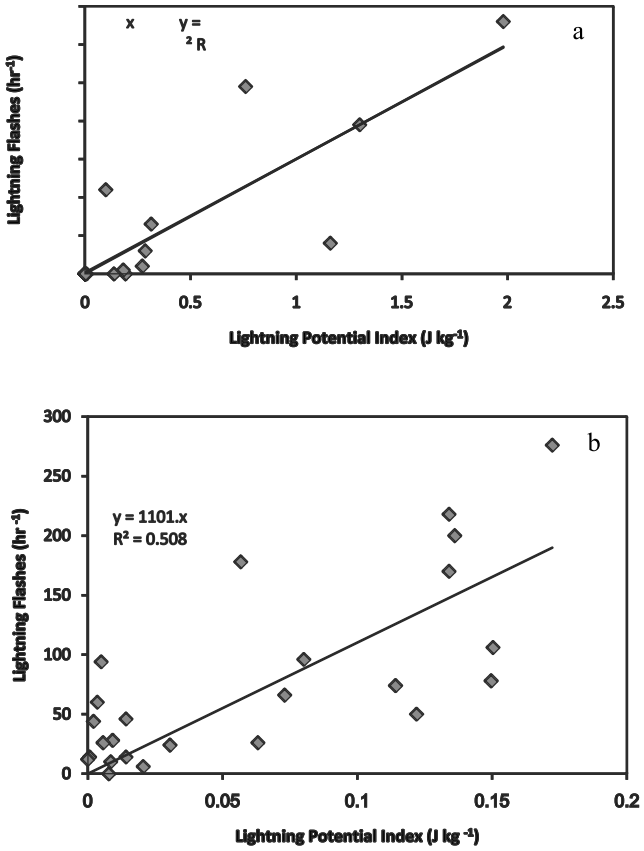

Figure 6. Number of lightning flashes in the appropriate areas for the two Israeli case studies, (a) Afula and (b) Wadi, versus the average WRF-computed LPI. The graphs were obtained after aligning the data such that the peak occurrence time of the observed lightning corresponded to the peak time at which the maximum in the curve of the average potential index occurred. The 15 min lightning and LPI data were also averaged over 30 min time intervals for the correlation graph.

included a coarse 27 km grid and three nests at 9, 3, and 1 km grid resolution. An example of a set of model grids for one of the case studies included 80 × 80 grid points at 27 km grid resolution, 139 × 139 grid points at 9 km grid resolution, 190 × 190 grid points at 3 km grid resolution, and 226 × 238 grid points at 1 km grid resolution (note that the exact setup of the model grids varied from case study to case study). The model was run using a 162 s time step on the outer 27 km grid, which then decreased to 3 s on the 1 km grid.

[13] We used rapid radiative transfer model long-wave radiation [*Mlawer et al.*, 1997] with the Dudhia shortwave radiation scheme [*Dudhia*, 1989]. The Monin-Obukhov (Janjic) scheme [*Janjic*, 1996] was used to simulate surface layer fluxes, whereas the Mellor-Yamada-Janjic turbulent kinetic energy (TKE) scheme [*Mellor and Yamada*, 1982; *Janjic*, 1990, 1994] was used to simulate boundary layer fluxes. The land surface fluxes were obtained with the NOAA land surface model (see *Chen and Dudhia* [2001] and as modified by *Liu et al.* [2006]). The Kain-Fritsch [*Kain and Fritsch*, 1993] new Eta scheme was used on the 27 and 9 km grids to parameterize moist convection. The 3 and 1 km grids used the Thompson microphysical scheme [*Thompson et al.*, 2004]. The model was initialized using reanalysis data from the Global Forecast Systems model. The model simulation duration ranged between 18 and 36 h, depending on the experimental case. It is considered that the model needs at least 6 h to ''spin up,'' so for the evaluation of the presented methodology, model outputs after t + 6 h have been used.

2.3. Lightning Data

[14] We used two sources for the lightning data: the Israeli Electrical Company LPATS system, which covers a range of 500 km from central Israel, and the ZEUS European network, which has good coverage of the central and western Mediterranean. ZEUS is a long-range lightning detection network with receivers located at six sites in Europe (Birmingham, United Kingdom; Roskilde, Denmark; Iasi, Rumania; Larnaca, Cyprus; Athens, Greece; and Lisbon, Portugal). The ZEUS receivers record the radio noise (sferics) emitted by CG and IC lightning discharges in the very low frequency (between 7 and 15 kHz). At each receiver site, an identification algorithm is executed that detects a probable sferics candidate, excludes weak signal and noise, and is capable of capturing up to ∼70 sferics per second. Then the lightning location is retrieved (at the central station of the network) using the arrival time difference triangulation technique. The location accuracy of ZEUS, compared to the LINET lightning detection network [*Betz et al.*, 2004] over Central Europe, has shown that the characteristic location error of ZEUS is of the order of 4–5 km over the study area [*Lagouvardos et al.*, 2008, 2009]. Further details on the ZEUS network are give by *Kotroni and Lagouvardos* [2008].

[15] For the Israeli case studies, we used CG lightning locations obtained from the Israel Electric Corporation LPATS [see *MacGorman and Rust*, 1998, section 6.10], an array that includes eight LF antennas dispersed all over the country. The system uses the difference in time-of-arrival technique for locating lightning strokes and supplies information on the time and location, polarity, and peak current of CG lightning flashes (IC discharges are not registered) that occur in Israel and up to 500 km from its borders. The temporal resolution of the LPATS is ∼15 ms, the position accuracy within the network coverage is ∼500 m, and the detection efficiency is stated at the 90% level of CG lightning flashes. Operationally, this system misses IC activity, and hence, the total number of flashes reported in the various case studies in Israel is significantly lower.

3. Case Study Simulations

[16] We used the FLASH project database (http://www.flashproject.org/) of Mediterranean storms to investigate the performance of the LPI against observed lightning and to evaluate the evolution of precipitation fields as predicted by the WRF model against radar- and rain-gauge-derived amounts (where available). The lightning flash data were gridded in 1 km boxes within the simulation area and accumulated over time. Figure 1 displays the geographical location of the case study domains across the Mediterranean. We conducted several sensitivity studies evaluating

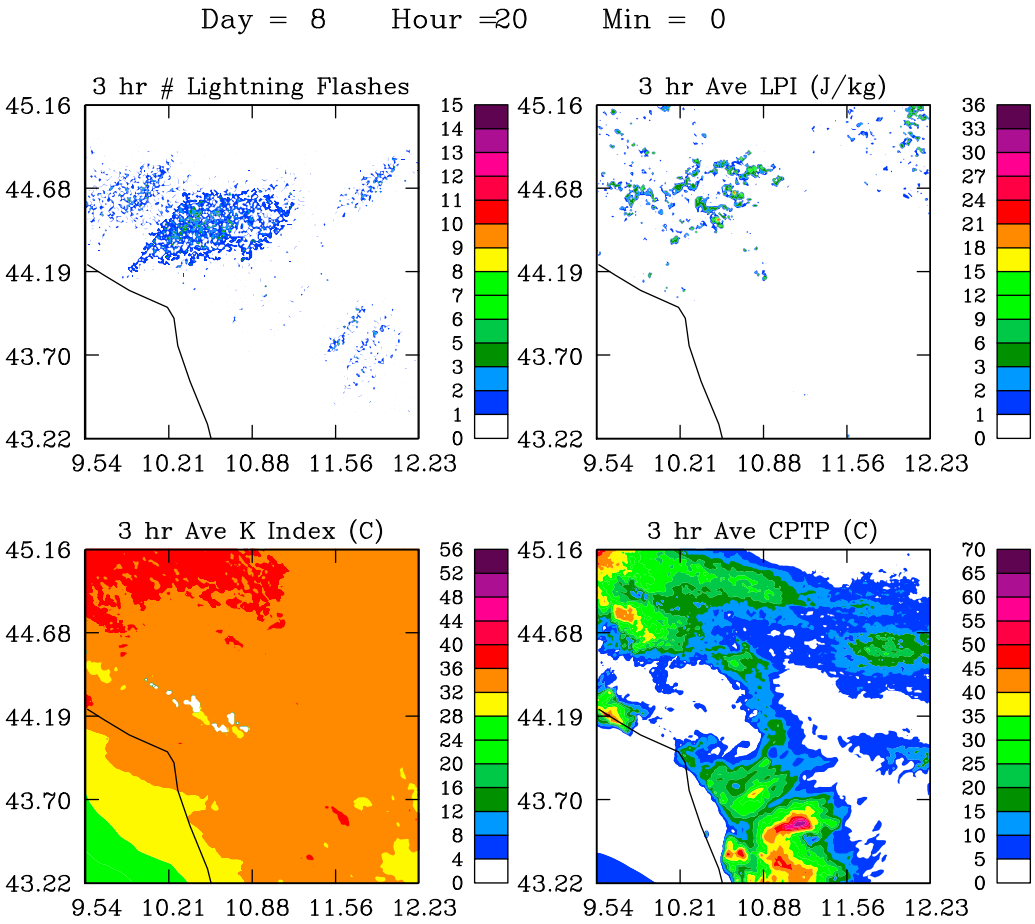

Figure 7. Three hour averages of observed lightning and predicted LPI, K index, and CPTP for 1500–1800 UTC on 8 September 2006 (for northwestern Italy).

sensitivity of the LPI to the depth of the charging zone and found that there were no significant and consistent differences for different depths. In some case studies, a deeper charging zone (until −40°C) slightly improved the correlation between the LPI and observed lightning; however, in other cases, it lowered it slightly. This probably reflects the fact that the main charging potential resides in the 0°C to −20°C region.

3.1. Afula, Israel, 28 October 2006

[17] A surface Red Sea trough penetrated into the Mediterranean Sea and developed a closed, but shallow, cyclone north of Israel. Rain occurred late on 27 October and during the early morning hours of the following day. The storm produced precipitation in several locations along the coastline and inland, with some locations receiving short periods of intense rain that culminated in flash flooding. This system was accompanied by weak electrical activity, concentrated in a few cells and for a rather short period of time. Although there is an ∼25 km northeast offset between the location of the maximum LPI and the place where the actual CG lightning activity was observed, the general characteristics of the activity were very well reproduced, and the broken and isolated nature of the convection is indicated. The spatial offset between the predicted and observed locations of the high electrical activity implies that we could have expected a parallel shift in the location of the heavy convective rainfall. Since lightning data are available in real time, this offset can be used to better predict the near-term occurrence of heavy convective rain, allowing for improved nowcasting.

[18] In Figure 2, we plotted area-averaged values of observed lightning and LPI over several hours against the observed and WRF-simulated rainfall for the same time period. The averages are done over areas ∼100 × 100 km^2. Averaging over an area of this size allows us to compare measured versus computed model outputs, even though there was some displacement of the simulated precipitation field from the observed. In the Afula flood case, the curve showing the number of observed CG lightning flashes versus time peaked sharply at ∼0800 UTC, whereas the precipitation peaked almost an hour later at ∼0900 UTC (Figure 2a). Likewise, in the WRF simulation, the LPI peaked sharply at ∼0900 UTC, which was followed thereafter by a peak in the WRF-simulated precipitation at 1000 UTC (Figure 2b). Hence, the time dependence of the WRF precipitation (and, by extension, the LPI) is well predicted, notwithstanding the displacement in time from the actual observations. Moreover, the WRF-predicted accumulated rainfall of 45.9 mm is in good agreement with the area-averaged radar observed precipitation of 53.9 mm.

[19] The possible relevance of the LPI in evaluating the potential for heavy rain is demonstrated in Figure 3. Figures 3a and 3b show the number of observed lightning

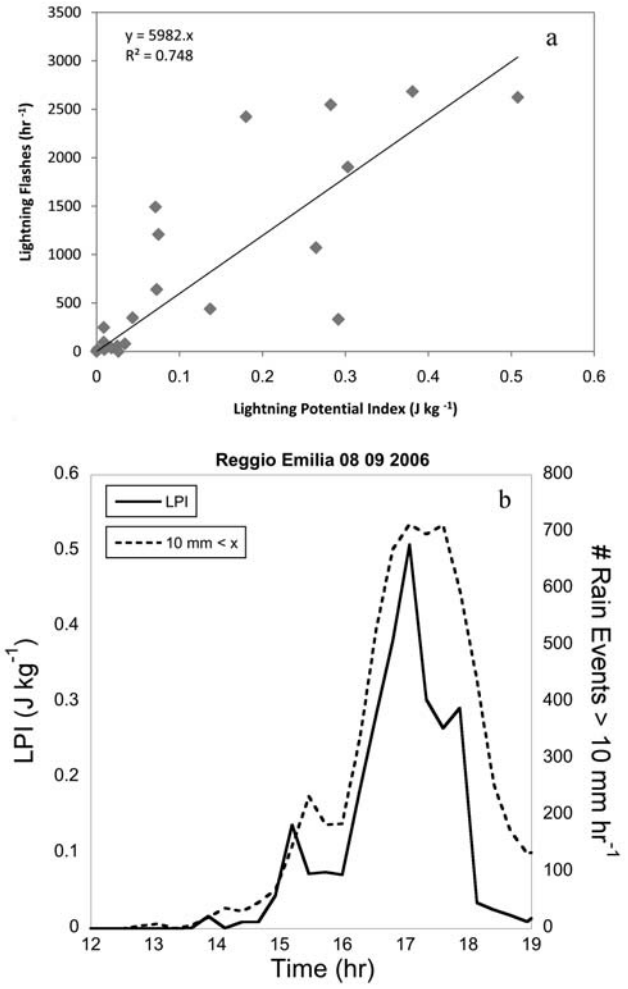

Figure 8. WRF-computed LPI (a) plotted as a function of time against the number of WRF rain events >10 mm h^{-1} for the area around Emilia Romagna, Italy, and (b) averaged and plotted against the number of lightning flashes in the region obtained after aligning the data as in Figure 6.

flashes versus time against the number of rain events (RE), where a rain event is defined as model accumulated rain within a 1 × 1 km model grid element. We plotted RE values greater than 10 mm h^{-1} and the number of events where 1 < RE < 5 mm h^{-1}. Figure 3 shows the existence of a "scale separation" in this case study, consisting of convective and stratiform rain regimes. The convective rain episode (RE > 10 mm h^{-1}) follows, with a small time delay, the time evolution of the number of lightning flashes. In comparison, the number of widespread stratiform-type rain events (1 < RE < 5 mm h^{-1}) presents a much flatter curve that reaches a maximum several hours after the peak in the convective rain and does not coincide with lightning activity. Figure 4a shows the average model calculated LPI versus the number of simulated RE > 10 mm h^{-1}, and Figure 4b shows the LPI versus time against 1 < RE < 5 mm h^{-1}. The WRF model results exhibit the same scale separation, although the model does not well simulate the tail in the distribution of the stratiform-type rain and, as a result, underestimates the rain compared with the measurements, a common problem with bulk schemes.

3.2. Wadi Ara, Israel, 1–2 April 2006

[20] This storm was characterized by enhanced convection resulting from mesoscale features; relatively high moisture content within the midtropospheric layers that originated from central Saudi Arabia, with additional humidity acquired from the Mediterranean Sea; and intensive upward motion coinciding with the warm conveyor belt of the cyclone. These atmospheric conditions caused high rain amounts over relatively small areas, resulting in severe flooding, serious damage to agriculture and infrastructure, and loss of lives [*Morin et al.*, 2007]. Figure 5 shows the 3 h integrated observed lightning activity and the predicted average values of the LPI, KI, and CPTP for 2 April 2006 over central Israel, between 0600 and 0900 UTC. While the KI and CPTP only give a broad and general indication of where lightning activity may be possible, the LPI closely matches the spatial distribution of the actual observed CG lightning in one of the predicted heavy rainbands. The second and northern line of predicted high LPI values was not evident in the observed lightning activity, suggesting that the model may have overpredicted the intensity of convection in that region. Again, the LPI offers a tool for real-time adjustment of heavy rain prediction, by comparing the location of the observed lightning activity with the LPI. Moreover, the LPI gives a much more localized prediction of where to expect convective cloud development and lightning compared to the KI and the CPTP. Since these last indices are distinct from the microphysical fields, they indicate the potential for lightning even in areas where there was no model precipitation and thus seem to be much less useful for accurate prediction of lightning activity. This stresses the advantage of a charging-potential-based lightning index over other indices such as KI and CPTP.

[21] When the WRF model predicts convection in a certain region, it appears that the LPI is a useful predictor for the potential for lightning. To verify this, the 15 min lightning data and LPI values were averaged over 30 min. Then, the data were aligned such that the maximum number of lightning observations occurred when the WRF model computed the maximum in the LPI. The two data sets were then plotted against each other. The correlation was 0.74 in the Afula case (Figure 6a) and 0.51 in the Wadi Ara case (Figure 6b).

3.3. Emilia Romagna, Italy, 8 September 2006

[22] An intense anticyclone over Great Britain carried a cold front to northern Italy. This cold advection caused a general cooling of the middle troposphere, thus destabilizing it. Large diurnal warming of the surface layer where the temperature rose by 6°C–7°C led to further destabilization of the atmosphere. Ultimately, this prolonged surface warming triggered deep and large convection that rapidly developed during midday, resulting in severe lightning activity, precipitation, and flooding. Figure 7 shows the 3 h averages of the observed lightning activity and the predicted values of the LPI, KI, and CPTP for 8 September 2006 over northern Italy, between 1500 and 1800 UTC. The KI and CPTP miss the actual location of convective activity. Furthermore, they indicate broad regions prone to convective activity and, consequently, wider regions with a high probability for lightning activity, where, in reality, there was none. The spatial "false alarm" that may arise from such

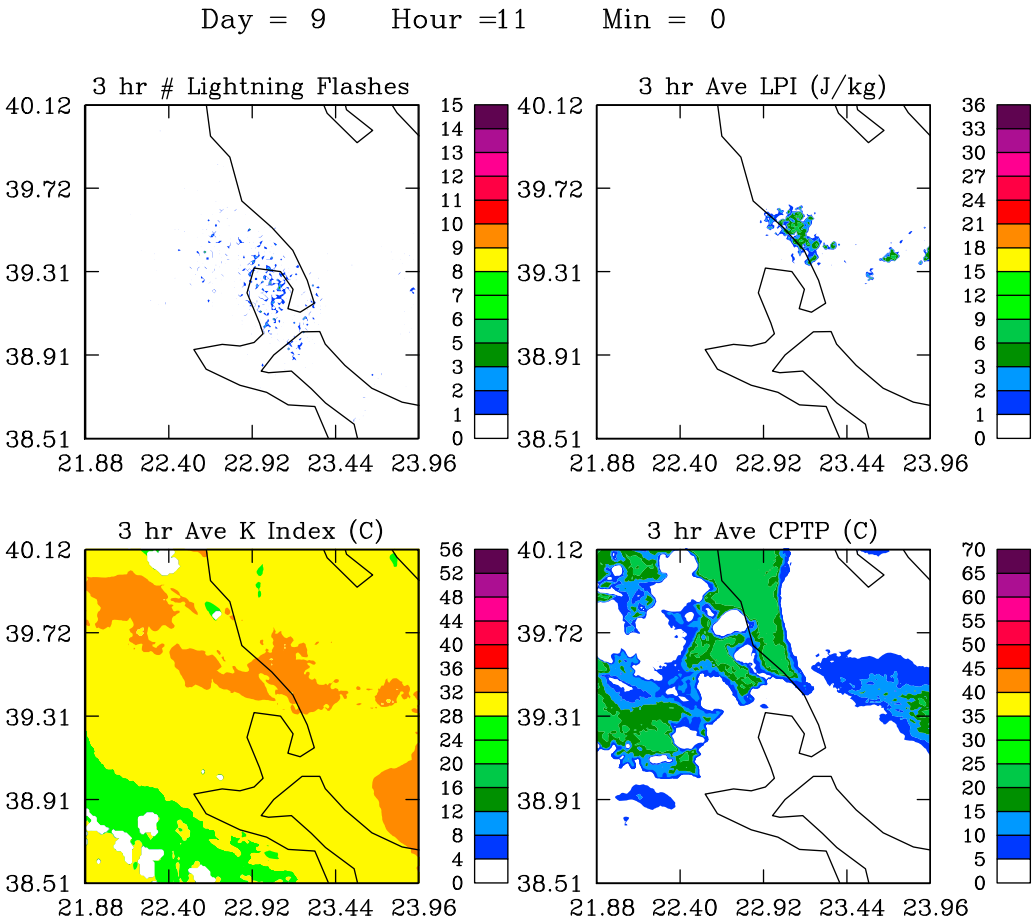

Figure 9. Three hour averages of ZEUS system-detected lightning and predicted LPI, K index, and CPTP for 0600-0900 UTC on 9 October 2006 (for central Greece).

broad indices is minimized when using the LPI, which gives a more localized and accurate distribution of regions prone to convective activity and lightning.

[23] The simulation results obtained for the Emilia Romagna case were qualitatively similar to those obtained for the Afula case (3.1). For instance, the WRF power index peaked sharply at 1700 UTC, while the number of rain events greater than 10 mm h^{-1} peaked at 1800 UTC (Figure 8a). Likewise, there is a high correlation between potential index and the number of observed flashes (Figure 8b). The number of observed flashes by the ZEUS network within a 100 × 100 km^2 area centered on the area of flooding was >3000, compared to only about 140 in the Afula case. The amount of observed lightning by the ZEUS system is clearly larger compared to the Israeli case, probably because it also includes IC flashes, whereas the former includes only CG flashes. This can partly explain why similar values of LPI correspond to different amounts of lightning flashes.

3.4. Volos, Greece, 9–11 October 2006

[24] A low-pressure system of 1008 mbar, centered over the Aegean Sea and associated with a cold front, affected the area of Greece on 9 October 2006. The surface system was associated with a 500 hPa cutoff low over the Ionian Sea that was moving very slowly southeastward without further deepening. Regarding lightning activity, on 9 October 2006 it was significant primarily on the west coast of Greece but also over central Greece and especially over the area of Volos, where a very high value of rainfall (∼230 mm) was recorded within an ∼12 h period.

[25] Figure 9 presents the 3 h averages of the observed lightning activity by the ZEUS network on 9 October between 0600 and 0900 UTC and the predicted values of the LPI, KI, and CPTP for this event. As in previous cases, the KI and CPTP missed the actual location of convective/lightning activity and indicated a much broader region with high probability for lightning occurrence (>50%) when actually there was none. The LPI simulated quite well the spatial extent of the lightning, although the position was offset by several tens of kilometers.

[26] In the Volos case, the temporal evolution of the WRF-simulated LPI was similar to the temporal evolution of the observed lightning, until about 1600 UTC on 9 October 2006 (Figure 10a). After 1600 UTC, the number of observed lightning flashes decreased to zero (∼1800 UTC), while the WRF continued to simulate relatively large values of the LPI. The maximum average values of the LPI simulated by WRF were ∼0.3 J kg^{-1}, a value that is about 30% of the values simulated in the Afula case study, but this was probably due to the relatively small area coverage of the lightning, rather than the model under-predicting the actual amount of convection. Moreover, the LPI remained close to 0.3 J kg^{-1} for many hours, and the time period over which there were more than 1000 rain events greater than 10 mm h^{-1}

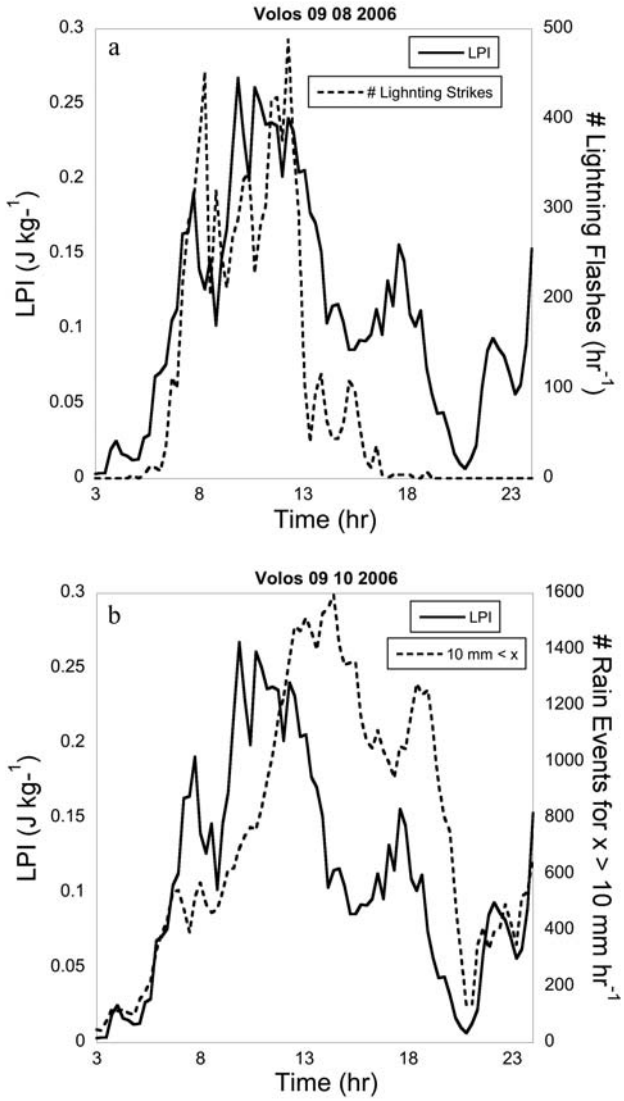

Figure 10. (a) The WRF average LPI and number of lightning flashes versus time for the area around Volos, Greece. (b) The WRF LPI versus time plotted against the number of WRF rain events >10 mm h^{-1}. The bounding box was between 22.42°E and 23.42°E, 38.83°N and 38.93°N.

was also comparatively long (Figure 10b). It should be noted that the LPI also properly depicted the relative reintensification of lightning activity around 2200 UTC, after the minimum observed around 2030 UTC.

[27] Figure 11 shows the relation between the observed lightning and the LPI. The data sets were again aligned, and the LPI time series was truncated to eliminate LPI values >0 when the lightning observations were 0. The number of CG lightning flashes peaked at ~450 h^{-1}, and the power index peaked near 0.18 J kg^{-1}. The correlation between the LPI and observed lightning was 0.71 for the time interval from 0300 to 1600 UTC on 9 October 2006.

3.5. Barcelona, Spain, 11–13 October 2005

[28] *Barrera et al.* [2007] studied this case in detail. The synoptic setting was such that a blocking high-pressure anticyclone centered over eastern Russia forced a trough that was formed near the coast of Portugal to move toward the southeast, reaching the center of the Iberian Peninsula in the form of a very well defined cutoff low on 13 October at 1200 UTC. This configuration generated a robust advection of warm and moist air masses against the mountain ranges of Catalonia at low levels. The event started on 11 October, but the heaviest rainfall was recorded on 13 and 14 October.

[29] In the 40 × 40 km^2 area around Barcelona, the heavy rain was measured before the onset of lightning, and there were only a few flashes detected by the ZEUS network (Figure 12) after the episode of the heaviest rain. Comparing the time-dependent average station rainfall with the WRF-simulated rainfall amounts shows that the WRF simulated the area-averaged rainfall quite well, although there is an offset in timing and the simulated rainfall peaks a couple of hours before the peak in measured rainfall. Even though the amount of simulated rain was quite large (similar to the observed), the LPI values, like the number of lightning flashes, were relatively small. Hence, the WRF-calculated LPI values did not appear to predict convection (or lightning), as the rain that fell was mostly caused by stratiform precipitation [*Barrera et al.*, 2007].

[30] Figure 13 presents the spatial distribution of observed lightning activity by the ZEUS network in the 3 h period between 0000 and 0300 UTC on 13 October 2005 in the region around the northeastern coast of Catalonia, near Barcelona. Clearly, the KI and CPTP overpredict the spatial extent of areas with a possibility of lightning, and the predicted areas for high lightning probability are offset to the south, namely, above the Mediterranean Sea. The LPI suggests that lightning should occur only over isolated areas, mainly over land, but with a slight shift to the west compared to where the ZEUS system actually detected lightning at that time interval. The results shown in Figure 13 were typical of those obtained in other 3- hourly time periods during the model simulation, which was done for the entire duration of this flash flood event.

4. Summary and Conclusions

[31] In this work, we introduced the lightning potential index (LPI), which is a measure of the potential for charge

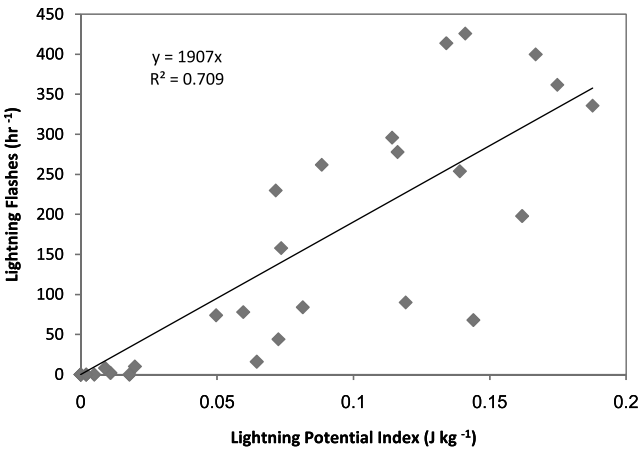

Figure 11. The number of observed lightning flashes versus the WRF-calculated LPI for the Volos, Greece, case study. The lightning data were aligned as in Figure 6.

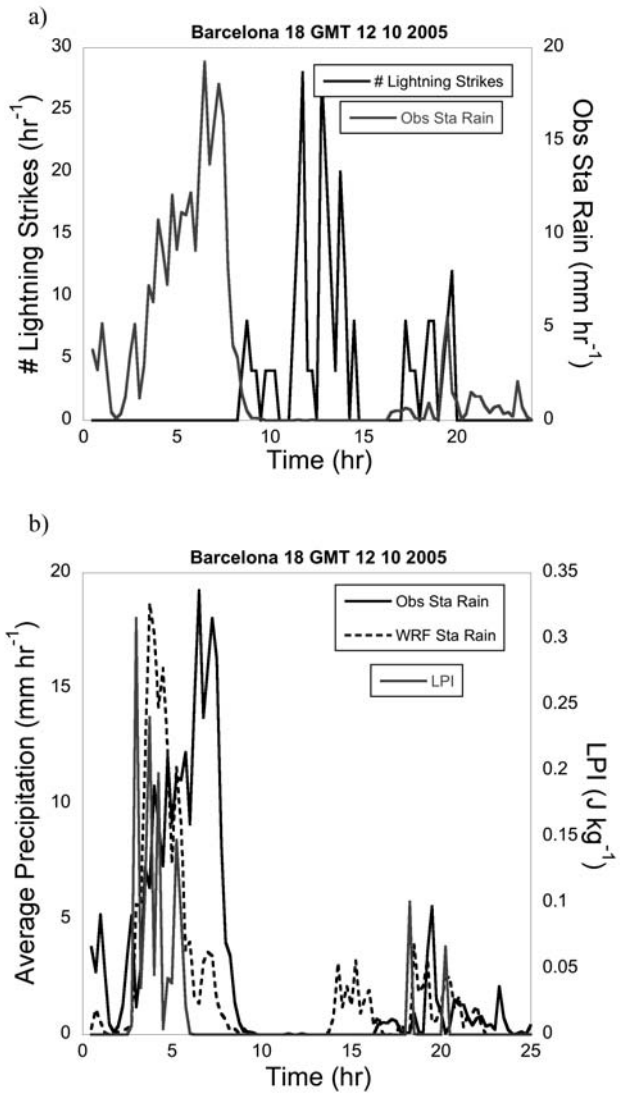

Figure 12. (a) The number of lightning flashes versus time against the observed (average) station rainfall for an area around Barcelona, Spain. (b) The WRF simulation of average rainfall interpolated to the location of station observations versus time plotted against observed rainfall. Also shown is the WRF simulation of LPI versus time in the same graph. The data were averaged over the bounding area 1.98°E and 2.28°E; 41.18°N and 41.48°N (∼30 km).

generation and separation that leads to lightning flashes in convective thunderstorms. The aim of this work was to investigate the potential for this index to be used for predicting lightning density in a way that reflects the capability of present-day numerical weather prediction models to properly describe cloud and precipitation fields. The numerical experiments were used to investigate the relationship between the model-derived LPI and the observed cloud-to-ground lightning activity. The superiority of the LPI against thermodynamic indices for lightning prediction, such as the KI and CPTP, was clearly demonstrated for these case studies.

[32] The model reproduced the general characteristics of convection, including precipitation amounts, but not always the specific location of convection and the accurate time of its commencement. When averaged over a 100 × 100 km^2 area, there was a high correlation between the LPI and observed lightning activity, as well as of the maximum LPI values and maximum simulated rainfall. In the cases when the ZEUS data were used, the lightning data points present a substantial part of the total lightning activity (IC + CG) that occurred. It is known that at the initial stages of electrical activity, intracloud flashes dominate the total lightning, and cloud-to-ground flashes only appear at a later stage [*Williams et al.*, 1989; *Maier and Krider*, 1986], and so we can safely assume that the observed activity correctly reflects the total lightning activity, within the limit of the network detection level and overall performance at specific regions. Furthermore, we suggest that since the LPI is derived from the same microphysical fields that eventually produce model precipitation, in principle, the use of the LPI, in conjunction with real-time lightning observations, can aid in the prediction of the onset of heavy convective rain.

[33] *Jessup and DeGaetano* [2008] compared the properties of flash flooding and nonflooding events in portions of New York and Pennsylvania. They noted that several parameters, e.g., atmospheric moisture and various convection indices, were useful in separating heavy rain events from climatology. These parameters indicate the potential for heavy rain, but they found that antecedent soil moisture was the most skillful predictor of flash flood occurrence prior to the occurrence of heavy rain. They also found that flash flooding was more likely with relatively small to moderate CAPE and suggested that flash flooding can occur when there are primarily collision-coalescence warm rain processes. Hence, the flash floods they described were probably caused by large-scale moisture advection, similar to the Barcelona case study presented in section 3.5. Our study, in contrast, highlights the potential for flash flooding from convective storms that have significant amounts of mixed phased hydrometeors, which are usually associated with high values of lightning activity. Recently, *Casati and Wilson* [2007] described a new spatial-scale decomposition of the ''Brier score'' and applied their approach to verification of lightning probability forecasts using lightning forecasts from the Canadian Meteorological Center (CMC). These forecasts provide the probability that the number of lightning flashes in a 3 h period exceeds some specified thresholds. Forecasts are produced at ∼24 km grid resolution, out to 48 h. The CMC lightning probability forecasts exhibit the largest error on the smallest scales, and the percentage of error for intense lightning activity is larger on small scales than for modest lightning activity. In fact, the CMC forecasts exhibited positive skill on scales greater than 700 km and negative skill on scales smaller than 400 km. The utilization of explicit cloud models will hopefully reduce the scale at which lightning forecasts become useful, perhaps to ranges of tens of kilometers. For instance, *Roberts and Lean* [2008, p. 95] concluded from their analysis that 1 km simulations are ''capable of a significant improvement in rainfall prediction over scales [i.e., river catchments] that are useful for flood prediction, even if skill close to the grid-scale is low.'' They also anticipated that data assimilation would further improve skill particularly over the first few hours of simulation when spin-up from a coarse resolution state can be a problem.

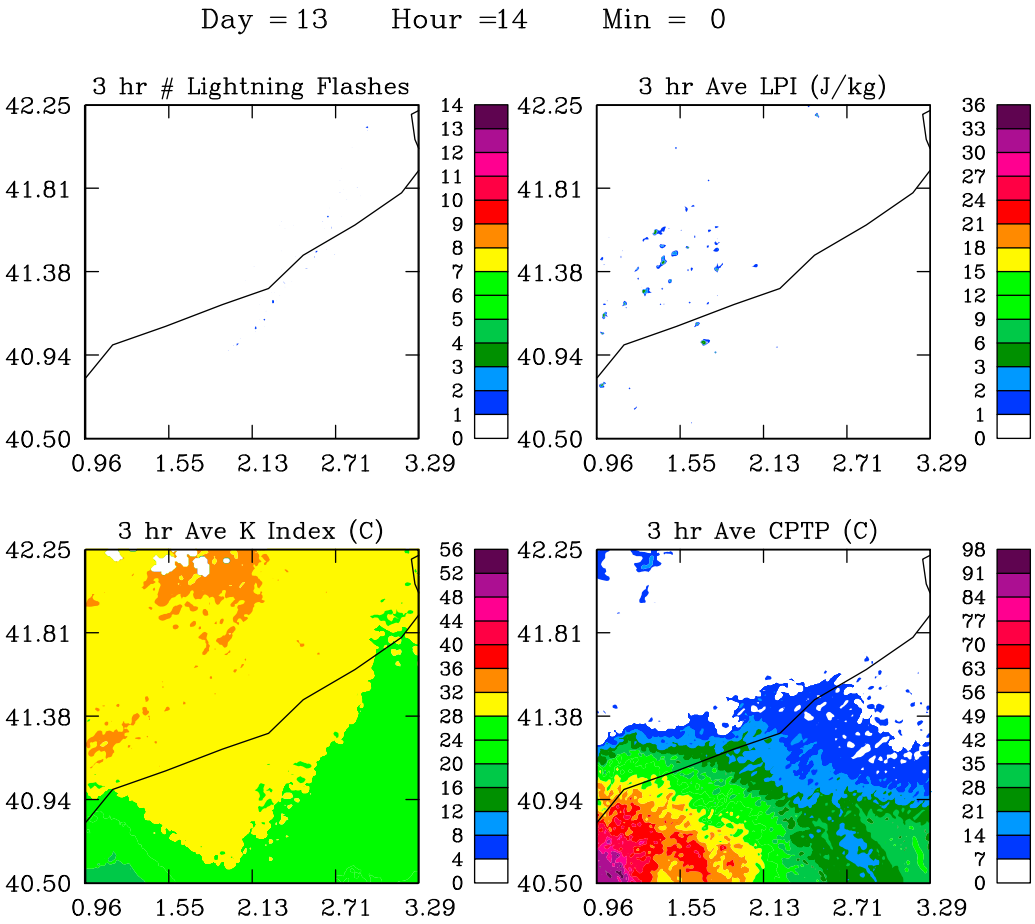

Figure 13. Three hour averages of observed lightning (by ZEUS) and predicted LPI, K index, and CPTP for 0000–0300 UTC on 13 October 2005 (for the northeastern coastal region of Catalonia near Barcelona).

[34] One way to address the difficulty of predicting localized convection would be to use an ensemble forecast. At this stage in the development of computer resources, this would be limited to simulations with 3 km grid resolution (which is not always adequate to initiate convection at the correct time, let alone correct place). If an ensemble system were employed, one could evaluate the forecasts using a method similar to that of *Ferro* [2007], who describes an approach for verifying deterministic forecasts of rare, extreme events. One could also use observed lightning to evaluate which ensemble member is most likely to verify against observations. If the observed lightning coverage is consistent with one (or more) of the member's forecasted LPI, then one might have greater confidence in that ensemble member's model forecasted rainfall amounts, thus providing important information to the forecaster in his prediction of the potential for flash flooding.

Appendix A

[35] The thunderstorm potential based on the critical values of KI, according to *Sturtevant* [1995], defines the probability in percentage for occurrence. The thunderstorm potential for the different values of KI is as follows: 0% for KI = 0–15; 20% or unlikely for KI = 18–19; a 35% potential, or an isolated thunderstorm, for KI = 20–25; 50% potential or widely scattered thunderstorms for KI = 26–29; 85% potential or numerous thunderstorms for KI = 30–35; and 100% (certain) chance for thunderstorms for KI values > 36. Lifted index (LI) values and the risk of thunderstorms and severe weather activity are: LI > 2, no significant activity; 0 < LI < 2, showers/thunderstorms possible (additional lift needed); −2 < LI < 0, thunderstorms possible; −4 < LI < −2, thunderstorms more probable, but few, if any severe; and LI < −4, severe thunderstorms possible.

[36] **Acknowledgments.** This research was conducted in the framework of the FLASH project, contract 036852 of the EU 6th framework program. We thank Aitor Atencia for his contribution in the Barcelona case analysis and Baruch Ziv for helpful discussions.

References

Altaratz, O., Z. Levin, Y. Yair, and B. Ziv (2003), Lightning activity over land and sea on the eastern coast of the Mediterranean, *Mon. Weather Rev.*, *131*, 2060–2070, doi:10.1175/1520-0493(2003)131<2060:LAOLAS>2.0.CO;2.

Barrera, A., V. Altava-Ortiz, M. C. Llasat, and M. Barnolas (2007), Heavy rain prediction using deterministic and probabilistic models–the flash flood cases of 11–13 October 2005 in Catalonia (NE Spain), *Adv. Geosci.*, *12*, 121–126.

Betz, H.-D., K. Schmidt, P. Oettinger, and M. Wirz (2004), Lightning detection with 3-D discrimination of intracloud and cloud-to-ground discharges, *Geophys. Res. Lett.*, *31*, L11108, doi:10.1029/2004GL019821.

Bright, D. R., M. S. Wandishin, R. E. Jewell, and S. J. Weiss (2005), A physically based parameter for lightning prediction and its calibration in ensemble forecasts, paper presented at Conference on Meteorological Applications of Lightning Data, Am. Meteorol. Soc., San Diego, Calif.

Caranti, G. M., E. E. Avila, and M. A. Ré (1991), Charge transfer during individual collisions in ice growing from vapor deposition, *J. Geophys. Res.*, *96*(D8), 15,365–15,376, doi:10.1029/90JD02691.

Casati, B., and L. J. Wilson (2007), A new spatial-scale decomposition of the Brier score: Application to the verification of lightning probability forecasts, *Mon. Weather Rev.*, *135*, 3052–3069, doi:10.1175/MWR3442.1.

Chen, F., and J. Dudhia (2001), Coupling an advanced land-surface/hydrology model with the Penn State/NCAR MM5 modeling system. Part I: Model implementation and sensitivity, *Mon. Weather Rev.*, *129*, 569–585, doi:10.1175/1520-0493(2001)129<0569:CAALSH>2.0.CO;2.

Davis, R. S. (2001), Flash flood forecast and detection methods, in *Severe Convective Storms*, *Meteorol. Monogr.*, vol. 50, pp. 481–525, Am. Meteorol. Soc., Boston, Mass.

Defer, E., K. Lagouvardos, and V. Kotroni (2005), Lightning activity in the eastern Mediterranean region, *J. Geophys. Res.*, *110*, D24210, doi:10.1029/2004JD005710.

Deierling, W., and W. A. Petersen (2008), Total lightning activity as an indicator of updraft characteristics, *J. Geophys. Res.*, *113*, D16210, doi:10.1029/2007JD009598.

Deierling, W., W. A. Petersen, J. Latham, S. Ellis, and H. J. Christian (2008), The relationship between lightning activity and ice fluxes in thunderstorms, *J. Geophys. Res.*, *113*, D15210, doi:10.1029/2007JD009700.

Dudhia, J. (1989), Numerical study of convection observed during the winter monsoon experiment using a mesoscale two-dimensional model, *J. Atmos. Sci.*, *46*, 3077–3107, doi:10.1175/1520-0469(1989)046<3077:NSOCOD>2.0.CO;2.

Ferro, C. A. T. (2007), A probability model for verifying deterministic forecasts of extreme events, *Weather Forecast.*, *22*, 1089–1100, doi:10.1175/WAF1036.1.

Gibergans-Báguena, J., and M. C. Llasat (2007), Improvement of the analog forecasting method by using local thermodynamic data. Application to autumn precipitation in Catalonia, *Atmos. Res.*, *86*, 173–193, doi:10.1016/j.atmosres.2007.04.002.

Gungle, B., and E. P. Krider (2006), Cloud-to-ground lightning and surface rainfall in warm-season Florida thunderstorms, *J. Geophys. Res.*, *111*, D19203, doi:10.1029/2005JD006802.

Janjic, Z. (1990), The step-mountain coordinate: Physical package, *Mon. Weather Rev.*, *118*, 1429–1443, doi:10.1175/1520-0493(1990)118<1429:TSMCPP>2.0.CO;2.

Janjic, Z. (1994), The step-mountain eta coordinate model: Further development of the convection, viscous sublayer, and turbulent closure schemes, *Mon. Weather Rev.*, *122*, 927–945, doi:10.1175/1520-0493(1994)122<0927:TSMECM>2.0.CO;2.

Janjic, Z. (1996), The Mellor-Yamada level 2.5 scheme in the NCEP eta model, paper presented at 11th Conference on Numerical Weather Prediction, Am. Meteorol. Soc., Norfolk, Va., 19–23 Aug.

Jessup, S. M., and A. T. DeGaetano (2008), A statistical comparison of the properties of flash flooding and nonflooding precipitation events in portions of New York and Pennsylvania, *Weather Forecast.*, *23*, 114–130, doi:10.1175/2007WAF2006066.1.

Kain, J. S., and J. M. Fritsch (1993), Convective parameterization for mesoscale models: The Kain-Fritsch scheme, in *The Representation of Cumulus in Numerical Models*, *Meteorol. Monogr.*, *46*, 165–177.

Katsanos, D., K. Lagouvardos, V. Kotroni, and A. Argiriou (2007a), Combined analysis of rainfall and lightning data produced by mesoscale systems in the central and eastern Mediterranean, *Atmos. Res.*, *83*, 55–63, doi:10.1016/j.atmosres.2006.01.012.

Katsanos, D., K. Lagouvardos, V. Kotroni, and A. Argiriou (2007b), Relationship of lightning activity with microwave brightness temperatures and spaceborne radar reflectivity profiles in the central and eastern Mediterranean, *J. Appl. Meteorol. Climatol.*, *46*, 1901–1912.

Keith, W. D., and C. P. R. Saunders (1989), Charge transfer during multiple large ice crystal interactions with a riming, *J. Geophys. Res.*, *94*(D11), 13,103–13,106, doi:10.1029/JD094iD11p13103.

Kotroni, V., and K. Lagouvardos (2008), Lightning occurrence in relation with elevation, terrain slope and vegetation cover over the Mediterranean, *J. Geophys. Res.*, *113*, D21118, doi:10.1029/2008JD010605.

Lagouvardos, K., V. Kotroni, H. Betz, and K. Schmidt (2008), Assessment of the ZEUS lightning detection network over Europe by comparison with lightning data from LINET, paper presented at 10th Plinius Conference on Mediterranean Storms, Eur. Geosci. Union, Nicosia, Cyprus, 22–24 Sept.

Lagouvardos, K., V. Kotroni, H.-D. Betz, and K. Schmidt (2009), A comparison of lightning data provided by ZEUS and LINET networks over Western Europe, *Nat. Hazards Earth Syst. Sci.*, *9*, 1713–1717.

Land, T. L., and S. A. Rutledge (2002), Relationships between convective storm kinematics, precipitation, and lightning, *Mon. Weather Rev.*, *130*(10), 2492–2506, doi:10.1175/1520-0493.

Latham, J., A. M. Blyth, H. J. Christian Jr., W. Deierling, and A. M. Gadian (2003), Determination of precipitation rates and yields from lightning measurements, *J. Hydrol.*, *288*(1–2), 13–19, doi:10.1016/j.jhydrol.2003.11.009.

Liu, Y., F. Chen, T. Warner, and J. Basara (2006), Verification of a mesoscale data-assimilation and forecasting system for the Oklahoma City area during the joint urban 2003 project, *J. Appl. Meteorol. Climatol.*, *45*(7), 912–929, doi:10.1175/JAM2383.1.

Llasat, M. C. (2001), An objective classification of rainfall events on the basis of their convective features, application to rainfall intensity on the north east of Spain, *Int. J. Climatol.*, *21*, 1385–1400, doi:10.1002/joc.692.

Lynn, B. H., and Y. Yair (2008), Lightning power index: A new tool for predicting the lightning density and the potential for extreme rainfall, *Geophys. Res. Abstr.*, *10*, Abstract EGU2008-A-01571, sref:1607–7962/gra/EGU2008-A-01571.

MacGorman, D. R., and W. D. Rust (1998), *The Electrical Nature of Storms*, 422 pp.,Oxford Univ. Press, New York.

Maier, L. M., and E. P. Krider (1986), The charges that are deposited by cloud-to-ground lightning in Florida., *J. Geophys. Res.*, *91*, 13,275–13,289, doi:10.1029/JD091iD12p13275.

Mansell, E. R., D. R. MacGorman, C. L. Ziegler, and J. M. Straka (2005), Charge structure and lightning sensitivity in a simulated multicell thunderstorm, *J. Geophys. Res.*, *110*, D12101, doi:10.1029/2004JD005287.

Mason, B. L., and J. G. Dash (2000), Charge and mass transfer in ice-ice collisions: Experimental observations of a mechanism in thunderstorm electrification, *J. Geophys. Res.*, *105*(D8), 10,185–10,192, doi:10.1029/2000JD900104.

Mellor, G. L., and T. Yamada (1982), Development of a turbulence closure model for geophysical fluid problems, *Rev. Geophys. Space Phys.*, *20*, 851–875, doi:10.1029/RG020i004p00851.

Mlawer, E. J., S. J. Taubman, P. D. Brown, M. J. Iacono, and S. A. Clough (1997), Radiative transfer for inhomogeneous atmosphere: RRTM, a validated correlated-k model for the longwave, *J. Geophys. Res.*, *102*(D14), 16,663–16,682, doi:10.1029/97JD00237.

Morin, E., N. Harats, Y. Jacoby, S. Arbel, M. Getker, A. Arazi, T. Grodek, B. Ziv, and U. Dayan (2007), Studying the extremes: Hydrometeorological investigation of a flood-causing rainstorm over Israel, *Adv. Geosci.*, *12*, 107–114.

Petersen, W. A., and S. A. Rutledge (1998), On the relationship between cloud-to-ground lightning and convective rainfall, *J. Geophys. Res.*, *103*, 14,025–14,040, doi:10.1029/97JD02064.

Piepgrass, M. V., E. P. Krider, and C. B. Moore (1982), Lightning and surface rainfall during Florida thunderstorms, *J. Geophys. Res.*, *87*, 11,193–11,201, doi:10.1029/JC087iC13p11193.

Price, C., and B. Federmesser (2006), Lightning-rainfall in Mediterranean winter thunderstorms, *Geophys. Res. Lett.*, *33*, L07813, doi:10.1029/2005GL024794.

Roberts, N. M., and H. W. Lean (2008), Scale-selective verification of rainfall accumulations from high-resolution forecasts of convective events, *Mon. Weather Rev.*, *136*, 78–97, doi:10.1175/2007MWR2123.1.

Saunders, C. P. R. (2008), Charge separation mechanisms in clouds, *Space Sci. Rev.*, doi:10.1007/s11214-008-9345-0.

Saunders, C. P. R., and S. L. Peck (1998), Laboratory studies of the influence of the rime accretion rate on charge transfer during crystal/graupel collisions, *J. Geophys. Res.*, *103*(D12), 13,949–13,956, doi:10.1029/97JD02644.

Saunders, C. P. R., W. D. Keith, and R. P. Mitzeva (1991), The effect of liquid water on thunderstorm charging, *J. Geophys. Res.*, *96*(D6), 11,007–11,017, doi:10.1029/91JD00970.

Sherwood, S. C., V. T. J. Phillips, and J. S. Wettlhaufer (2006), Small ice crystals and the climatology of lightning, *Geophys. Res. Lett.*, *33*, L05804, doi:10.1029/2005GL025242.

Skamarock, W. C., et al. (2005), A description of the advanced research WRF version 2, *NCAR Tech. Note NCAR/TN–468+ST*, Natl. Cent. for Atmos. Res., Boulder, Colo. (Revised January 2007).

Soula, S., H. Sauvageot, G. Molinié, F. Mesnard, and S. Chauzy (1998), The CG lightning activity of a storm causing a flash-flood, *Geophys. Res. Lett.*, *25*, 1181–1184, doi:10.1029/98GL00517.

Sturtevant, J. S. (1995), *The Severe Local Storm Forecasting Primer*, 197 pp., Weather Scratch Meteorol. Serv., Florence, Ala.

Takahashi, T. (1978), Riming electrification as a charge generation mechanism in thunderstorms, *J. Atmos. Sci.*, *35*, 1536–1548, doi:10.1175/1520-0469(1978)035<1536:REAACG>2.0.CO;2.

Tapia, A., J. A. Smith, and M. Dixon (1998), Estimation of convective rainfall from lightning observations, *J. Appl. Meteorol.*, *37*, 1497–1509, doi:10.1175/1520-0450(1998)037<1497:EOCRFL>2.0.CO;2.

Thompson, G., R. M. Rasmussen, and K. Manning (2004), Explicit forecasts of winter precipitation using an improved bulk microphysics scheme. Part I: Description and sensitivity analysis, *Mon. Weather Rev.*, *132*, 519–542, doi:10.1175/1520-0493(2004)132<0519:EFOWPU>2.0.CO;2.

Williams, E. R., and N. Renno (1993), An analysis of the conditional instability of the tropical atmosphere, *Mon. Weather Rev.*, *121*, 21–36, doi:10.1175/1520-0493(1993)121<0021:AAOTCI>2.0.CO;2.

Williams, E. R., M. E. Weber, and R. E. Orville (1989), The relationship between lightning type and convective state of thunderclouds, *J. Geophys. Res.*, *94*, 13,213–13,220, doi:10.1029/JD094iD11p13213.

Zhou, Y., X. Qie, and S. Soula (2002), A study of the relationship between cloud-to-ground lightning and precipitation in the convective weather system in China, *Ann. Geophys.*, *20*, 107–113.

V. Kotroni and K. Lagouvardos, Institute of Environmental Research, National Observatory of Athens, Lofos Koufou, 15236-Penteli, Athens, Greece.

M. d. C. Llasat, Department of Astronomy and Meteorology, Faculty of Physics, University of Barcelona, Av. Diagonal 647, 7a planta, E-08028 Barcelona, Spain. (carmell@am.ub.es)

B. Lynn and Y. Yair, Department of Life and Natural Sciences, Open University, I University Road, Ra'anana 43107, Israel. (barry.h.lynn@gmail.com; yoavya@openu.ac.il)

E. Morin, Department of Geography, Hebrew University of Jerusalem, Mount Scopus, Jerusalem 91905, Israel. (msmorin@mscc.huji.ac.il)

A. Mugnai, ISAC, CNR, Via del Fosso del Cavaliere, 100, I-00133 Rome, Italy. (a.mugnai@isac.cnr.it)

C. Price, Department of Geophysics and Planetary Science, Tel-Aviv University, Ramat Aviv 69978, Israel. (cprice@flash.tau.ac.il)